Optimizing phosphorus diffusion for photovoltaic applications: Peak doping, inactive phosphorus, gettering, and contact formation

Hannes Wagner, Amir Dastgheib-Shirazi, Byungsul Min, Ashley E. Morishige, Michael Steyer, Giso Hahn, Carlos del Cañizo, Tonio Buonassisi, and Pietro P. Altermatt

The phosphosilicate glass (PSG), fabricated by tube furnace diffusion using a $POCl_3$ source, is widely used as a dopant source in the manufacturing of crystalline silicon solar cells. Although it has been a widely addressed research topic for a long time, there is still lack of a comprehensive understanding of aspects such as the growth, the chemical composition, possible phosphorus depletion, the resulting in-diffused phosphorus profiles, the gettering behavior in silicon, and finally the metal-contact formation. This paper addresses these different aspects simultaneously to further optimize process conditions for photovoltaic applications. To do so, a wide range of experimental data is used and combined with device and process simulations, leading to a more comprehensive interpretation. The results show that slight changes in the PSG process conditions can produce high-quality emitters. It is predicted that PSG processes at 860 °C for 60 min in combination with an etch-back and laser doping from PSG layer results in high-quality emitters with a peak dopant density $N_{peak} = 8.0 \times 10^{18}\,cm^{-3}$ and a junction depth $d_j = 0.4\,\mu m$, resulting in a sheet resistivity $\rho_{sh} = 380\ \Omega/sq$ and a saturation current-density J_0 below 10 fA/cm^2. With these properties, the $POCl_3$ process can compete with ion implantation or doped oxide approaches. *Published by AIP Publishing.* [http://dx.doi.org/10.1063/1.4949326]

I. INTRODUCTION

The *n*-type emitter of most crystalline *p*-type silicon solar cells is formed by phosphorus diffusion. A common P diffusion method is to expose Si wafers in a furnace at about 800–900 °C to an atmosphere of $POCl_3$ and O_2 (with N_2 as a carrier gas), forming a phosphosilicate glass (PSG) on the wafer surfaces. This process step is usually called predeposition, and the resulting PSG provides a source of P dopants that diffuse into the Si wafer. Most commonly, an additional process step, called drive-in, follows the predeposition, where the supply of dopant gases is disconnected, and P from the existing PSG diffuses further into the Si wafer.

To find optimum process conditions for photovoltaic applications, three different effects have to be considered. First, the in-diffusion of P from the PSG, and its presence in electrically active and inactive states in the Si wafer, which increases Shockley-Read-Hall (SRH) recombination. Second, the gettering of impurities in Si in the direction toward the PSG. Third, the metal contact formation of the P-rich Si region to the external circuit. These three effects can be described as follows.

P diffusion is usually performed at 800–900 °C. At this temperature the solubility limit of active P (the dopant concentration) in silicon is around $3 \times 10^{20}\,cm^{-3}$.[1] Because the PSG is a high-concentration P source, this solubility limit is usually exceeded; thus inactive P also diffuses[2] and may form P clusters and after prolonged high-temperature treatment even precipitates.[3–8] See Fig. 1 for an overview. As a result, two different profiles diffuse into Si, an electrically active P profile, which is the emitter creating the *p-n* junction in the p-type wafer, and an inactive P profile.[9] The inactive P in the form of interstitial P, clusters of P, and possibly SiP precipitates causes an increase in SRH recombination[10–12] and a decrease in the collection efficiency of photogenerated carriers in the Si solar cell. Consequently, reducing the inactive P concentration can increase solar cell performance. In Refs. 13 and 14 it is shown that the inactive P concentration can be lowered significantly by reducing the $POCl_3$ flow rates during the PSG process. In Ref. 13 this reduction in inactive P concentration has resulted in an increase of up to 10 mV in open-circuit voltage (V_{OC}) in a solar cell. Other approaches[15,16] show that etching the PSG and then performing a drive-in reduces the inactive P concentration significantly.

The $POCl_3$ and its PSG layer are technologically successful because impurities are not likely to enter the Si, because (i) their vapor pressure in the glassy matrix is lowered by the melting process and (ii) they are nearly immobile in the glass.[19] This is in contrast to other dopant sources, such as gases, vaporized liquids, spin-on liquids, and some

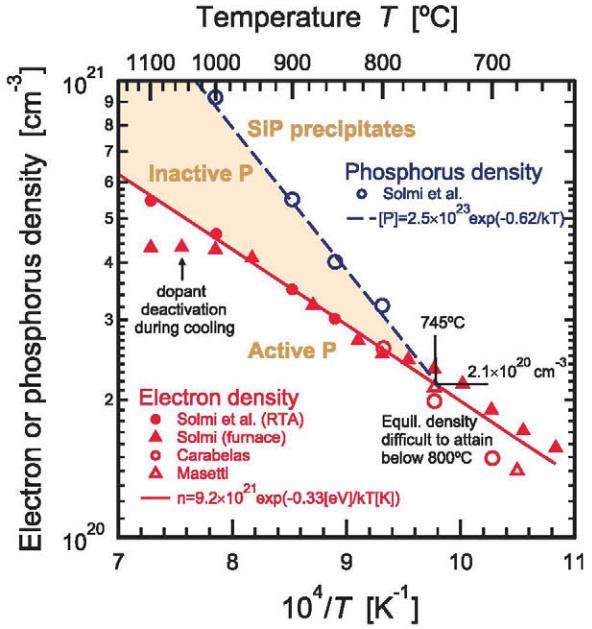

FIG. 1. Limit between activation of P (dopants) and inactive P (red solid line) as well as the solubility limit between inactive P and precipitating P (blue dashed line), as measured in thermal equilibrium in Refs. 2, 17, and 18.

other solid sources, where great care must be taken that impurities do not contaminate the Si. In turn, the PSG process is also essential for gettering of impurities from the Si bulk material,[20] which occurs at the same time and temperature conditions as the diffusion. The gettered impurities leave the base region and accumulate in the emitter region. Because the minority-carrier concentrations are lower in the emitter region than in the base region, the total amount of SRH recombination in the device is reduced. Further it may be possible that the impurities in the emitter are in a different phase (i.e., precipitated) which also reduces SRH recombination. Consequently, this improves the excess carrier lifetime in the base region. Especially for low-lifetime material, such as conventional multicrystalline silicon, this effect is essential to achieve higher bulk lifetimes. In Refs. 21–24 gettering of a variety of impurities in different Si materials is reported. Especially accumulation of Cu, Ni, Fe, and Cr in the emitter is shown.[22,23] In Ref. 25, it is shown that the gettering process conditions have to be adapted for high concentrations of Fe impurities. In general it can be followed that for a specific type of impurity and specific concentrations, individual PSG process conditions have to be adapted to maximize gettering efficiency. On the other hand, these process conditions must also create a high-quality emitter, requiring a low concentration of inactive P.

Screen-printing is conventionally used to contact a PSG-diffused emitter. In general, three different paths[26–29] exist for electron transport from Si via the contact to the external grid. First, direct current flow due to direct contact between Ag crystals and the grid. Second, tunneling through very thin PbO glass layers between Ag crystals and the grid. Third, current flow through the PbO glass layer by tunneling via metal impurities dispersed in the PbO glass layer. These transport mechanisms are assessed in Ref. 30.

Contacting a lowly doped emitter is reported to be difficult because the contact resistivity is high.[31,32] Another possible problem is that with decreasing P concentration, the in-diffused Ag profile can overcome the P profile and may shunt the emitter region.[28] Hence, in addition to high efficiency and metal impurity gettering, contact formation has to be considered when finding optimum process conditions for PSGs.

All three effects have their own optimum process conditions, but they are not independent from each other. This paper focuses on co-optimizing PSG formation for obtaining low saturation currents, effective gettering, and good contact formation. We start by showing optimized process conditions for forming the emitter, and then we show the limitations for gettering and contact formation. This strategy for identifying optimum process conditions can be adapted to other materials and more advanced process conditions.

II. PHOSPHORUS EMITTER IN SILICON

To understand the P emitter formed in silicon by the PSG, we discuss in this section the following fundamental issues in PSGs. First, the growth of a PSG to estimate its thickness. Second, how P moves within the PSG and the silicon crystal. Third, electrically active and inactive P in Si as a function of the $POCl_3$ flow. Fourth, possible depletion of P in PSG layers.

A. Growth model for the PSG layer

We will see in Secs. II B and III B that PSG layers rarely stay so thin that they become depleted of P during the drive-in. Hence, the PSG layer thickness x_{PSG} is not a critical parameter. However, the following quantitative model of x_{PSG} is viable for the etching of the PSG in advanced emitter structures, for optical inspection, and quality control in fabrication.

The PSG layer thickness x_{PSG} (including the SiO_2 layer at the interface between PSG and Si) depends on various process parameters such as deposition time t and deposition temperature T, the flows of N_2, $POCl_3$, and O_2, as well as the temperature of the $POCl_3$ bubbler $T_{bubbler}$. Typical thicknesses of PSGs are reported to be 10–80 nm.[13,33]

The growth behavior of the PSG layer obeys the parabolic law,[34] indicating that the rate controlling process is diffusion. To discuss the relative importance of the parameters describing the growth, we use a simple empirical equation for x_{PSG}, proposed by Negrini *et al.*[4]

$$\chi_{PSG} = \sqrt{B_0 \cdot \exp(-E_0/k_B T) \cdot t}, \quad (1)$$

where the constant E_0 is 1.7 eV, t the deposition time [min], T the deposition temperature [K] and the parameter B_0 [nm^2/min] empirically describes the influence of the gas flow rates on x_{PSG}. Unfortunately, B_0 cannot be given as a universal function of N_2, $POCl_3$, and O_2 flow rates.

To derive B_0 as a function of $POCl_3$ flow rate, we calibrate it on our experimental data for different PSG thicknesses $x_{PSG,Exp}$ published in Refs. 13, 33, and 35, where the $POCl_3$ flow rate was varied from 125 to 1500 sccm by

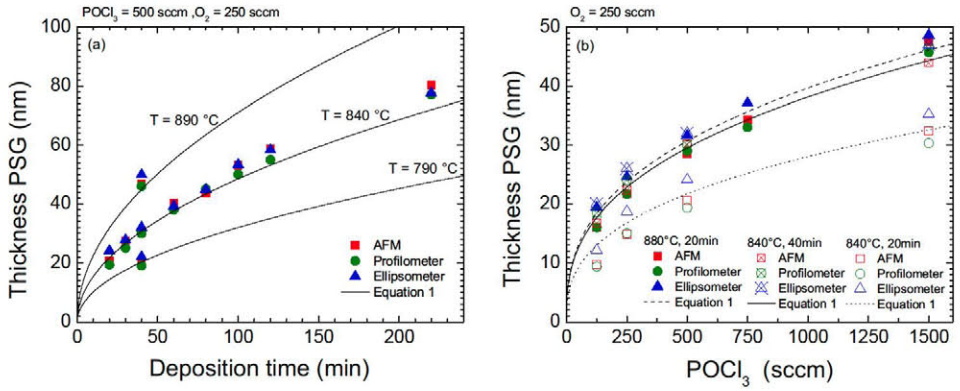

FIG. 2. Measured[13,33,35] and empirically fitted PSG thicknesses under various process conditions: (a) for different deposition times and temperatures, with constant N_2, $POCl_3$ and O_2 flows; and (b) for different $POCl_3$ flows, times, and temperatures, with constant N_2 and O_2 flows. The experimental values (symbols) are measured with different techniques, and the empirical fits (lines) are obtained with Eqs. (1) and (2).

holding the N_2 and O_2 flows constant. $x_{PSG,Exp}$ was measured with four different experimental techniques:[33] atomic force microscopy (AFM), profilometry, scanning electron microscopy (SEM), and spectroscopic ellipsometry. The measurement uncertainties were lowest (near 2 nm) for AFM and SEM and highest (4 nm) for the ellipsometer. From the calibration procedure we got the following expression for B_0 as a function of the $POCl_3$ flow Φ [sccm]

$$B_0 = a_1 \cdot (\sqrt{\Phi})^{a_2} \tag{2}$$

with $a_1 = 1.03561 \times 10^7$ [nm^2/min sccm$^{a2/2}$] and $a_2 = 1.51449$.

In a separate study,[35] we analyzed the influence of $x_{PSG,Exp}$ from the O_2 flow while keeping the $POCl_3$ flow constant. It was found that $x_{PSG,Exp}$ is rather independent of the O_2 flow: only for very small O_2 flows the formation of a PSG is suppressed, and for larger O_2 flows, x_{PSG} is influenced by only 1 nm (for flows up to 500 sccm).

Another parameter that might influence $x_{PSG,Exp}$ is the $POCl_3$ bubbler temperature $T_{bubbler}$. We varied in Ref. 36 $T_{bubbler}$ from 15.5 to 24.5 °C and found that the $x_{PSG,Exp}$ varies only by 4 nm. Because of this small influence we did not include the bubbler temperature in Eq. (1).

In Fig. 2 our experimental data from Refs. 13, 33, and 35 for $x_{PSG,Exp}$ and the calculated x_{PSG} from Eqs. (1) and (2) are presented. Overall a good fit of the experimental data can be obtained with Eqs. (1) and (2). Further improvements of a growth model may be achieved by taking N_2, O_2, and $T_{bubbler}$ into account.

B. Phosphorus in the PSG layer and in silicon

In Section II A it was shown that the PSG thickness is influenced by several process parameters, mainly by time, t, temperature, T, and the $POCl_3$ flow rate. These process parameters also influence the P diffusion in Si and within the PSG. The influence of t and T on the diffusion profile in Si has been investigated thoroughly (for a review, see Ref. 1). However, please note that such diffusion models of P within Si require the peak dopant density at the Si surface as input parameter and, accordingly, have limited predictive power. Therefore, we focus here on setting up a model that quantifies how the P profile is influenced directly by the $POCl_3$ flow. For a better knowledge of this dependence, the P flow within the PSG and through the interface to Si needs to be better understood, as is done in the following.

During the pre-deposition process, $POCl_3$ and O_2 accumulate on top of Si and create the PSG. After a PSG diffusion process, usually a layer structure described as PSG/SiO_2/Si is observed,[37] as shown in secondary ion mass spectrometry (SIMS) measurements shown in Fig. 3(a). The signal intensity of P is rather constant in the PSG, is minimal in the SiO_2 layer, and has a strong pile up at the interface between SiO_2 and Si.

The observed minimum of phosphorus in the SiO_2 layer can be explained as follows. On the one hand, the original Si surface is moved into the Si due to oxidation. On the other hand, a high segregation of P between SiO_2 and Si is reported.[38,39] This means that during the growth of the SiO_2 layer P is continuously pushed away from SiO_2 into the direction of Si. At the PSG/SiO_2 interface, instead, the situation is more complex. A possible explanation might be that segregation works in the direction of the PSG and diffusion in the direction of the SiO_2. It seems that both processes balance each other and as a result the observed minimum in the SiO_2 layer appears.

The strong pile-up at the SiO_2/Si interface can be explained as follows. Two processes are working in parallel: first, P is pushed into Si via segregation and second, P diffuses from the PSG/SiO_2 system in the direction of Si. The solubility limit of electrically active P is usually reached in Si and inactive P in various forms is observed.[2,3,5–8] This means that the overall P concentration is limited in Si and once this limit is achieved, P accumulates and piles up at the SiO_2/Si interface.

To analyze the influence of $POCl_3$ on phosphorus in the PSG/SiO_2/Si system, the $POCl_3$ flow was varied from 250 to 1000 sccm, while all other parameters were kept constant: $t = 40$ min, $T = 840$ °C, and $O_2 = 250$ sccm.[37] In Fig. 3(b) a small variation of P signal intensity in the PSG can be observed and a rather strong variation at the pile-up of P at the SiO_2/Si interface. This effect may be explained as follows. It is known[39] that the in-diffusion of P from the PSG in SiO_2 is stronger with a higher P content in PSG. This results in a higher content of P in the SiO_2 region and consequently a larger amount of diffused P from the SiO_2 into the Si. Finally, the solubility limit of P in Si is further exceeded and a stronger pile-up of P at the SiO_2/Si interface can be observed.

The previously described results explain why there is a variation in the amount of electrically active and inactive P

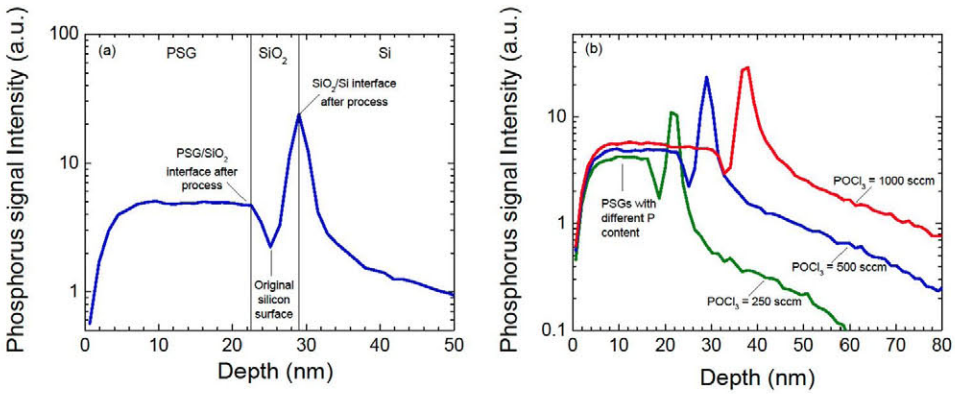

FIG. 3. SIMS measurements of phosphorus in the PSG/SiO_2/Si layer structure fabricated with different $POCl_3$ flows from Ref. 37. (a) SiO_2 layer between PSG and Si after 40 min of diffusion at 840 °C, with $POCl_3 = 500$ sccm and $O_2 = 250$ sccm. (b) Measurements on structures with the same process conditions as before, but different $POCl_3$ flows. A difference in P concentration is observable in the PSG layer and a stronger pile-up of P at the SiO_2/Si interface with higher $POCl_3$ flows. This leads to a stronger in-diffusion of inactive P into Si (cf. Fig. 4).

in Si. We analyzed the results in more detail for different $POCl_3$ flows.[13] In Fig. 4 SIMS measurements show the total amount of P in Si, and electrochemical capacitance voltage (ECV) measurements of the same samples show only the electrically active P concentration.[40] In this experiment four different $POCl_3$ flows were used while holding all other process parameters constant. The results show a decreasing inactive P profile (SIMS data) with decreasing $POCl_3$ flows, as can be explained with the discussion above. Compared with the SIMS data, the changes in electrically active P profile (ECV data) are less, because the temperature is kept constant and so is the solubility limit of P in Si. The P profile becomes shallower, but drops only for very low $POCl_3$ flows.

Note that in Fig. 4 the inactive P penetrates deeper into Si than the plateau at the solubility limit of the active P profile. This has been observed also in other laboratories,[14,41] but is not always the case.[16,42] Possible reasons for a deeper penetration of inactive P are: (i) the SIMS profile contain P clusters, which are stable and mobile. They are sufficiently stable, so they do not dissolve when diffusing deeper than the plateau of the solubility-limited active P; (ii) the SIMS profile contains very small precipitates, which do not dissolve quickly and therefore do not dissolve when diffusing into deeper regions where the solubility limit of P is not reached; these precipitates may form only during cool down of the samples while the solubility limit is lowered in an Arrhenius-like manner; (iii) the SIMS profile may contain large precipitates, which grow over time and penetrate more deeply into Si than the plateau. Under conventional process conditions in photovoltaics, usually no precipitates are formed, but the mobile clusters of interstitial phosphorus.

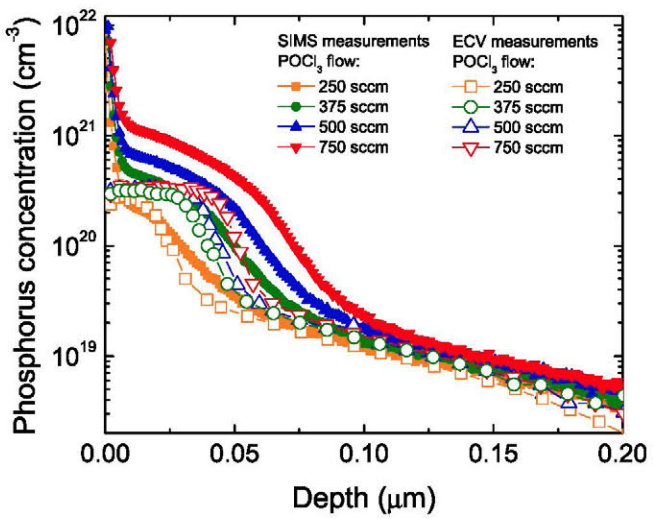

FIG. 4. The total P concentration in Si measured with SIMS (filled symbols) and the electrically active P concentration measured with ECV (empty symbols) for different $POCl_3$ flow rates. The profiles are obtained from PSG diffusions at 840 °C for 40 min with $O_2 = 250$ sccm and varied $POCl_3$ flows from Ref. 13. The calculation with the carrier mobility model from Refs. 43 and 44 leads to the sheet resistivities of 60, 70, 75, and 105 Ω/sq.

The above discussed ECV and SIMS measurements were taken on samples at room temperature after the PSG process. In Ref. 45 it is described that the PSG layer is viscous at process temperatures between 800 and 1200 °C. This means that during the process a liquid-like PSG could exist on top of SiO_2 and Si. It might be that also part of the SiO_2 may be viscous, because the viscosity of SiO_2 is strongly influenced by its P content and possibly by other elements like N, C, and H. Even under these conditions the above described diffusion processes still exist. The segregation from SiO_2 to a viscous PSG would also be strong, so does the diffusion from the high concentration PSG region to the low concentration SiO_2 region.

Another open question is whether the PSG's P content can be depleted during conventional process conditions. In Ref. 13 typical P doses in the PSG between 1 and 5 $\times 10^{16}\,cm^{-2}$ and doses in Si between 1 and 7 $\times 10^{15}\,cm^{-2}$ are reported. This means that after a conventional process of, e.g., 840 °C for 40 min, still a large amount of P remains in the PSG. It is questionable whether this amount can still diffuse into Si for two reasons. First, the strong pile-up of P at the SiO_2/Si interface may act like a diffusion barrier for P from the PSG. Second, the growing SiO_2 layer between PSG and Si may act like a diffusion barrier. We assume that a pure SiO_2 layer is sandwiched between the PSG layer and Si. Using a diffusivity model[46] for P in SiO_2, we simulate a process of 40 min at 840 °C with a peak concentration of 8 $\times 10^{21}\,cm^{-3}$ P atoms[13] at the PSG/SiO_2 interface: the concentration of P decreases to almost zero within the first 1 nm in SiO_2. This means that pure SiO_2 is an almost perfect diffusion barrier for P under the typically applied PSG process conditions. It seems likely that the growing SiO_2 layer during the PSG process begins to act as a diffusion barrier for P

from PSG in the direction of Si. Nevertheless the SiO_2 layer contains a high amount of P that can diffuse into Si.

III. PERC SOLAR CELL SIMULATION WITH ELECTRICALLY ACTIVE AND INACTIVE PHOSPHORUS PROFILES

As discussed above, it is well known that different process conditions for the PSG formation produce different electrically active P profiles (emitters) and different electrically inactive profiles in Si. It is evident that inactive P should be avoided for a high quality emitter to reduce SRH recombination. Further, the peak concentration of the electrically active profiles should be lowered to reduce Auger recombination. Considering the effects discussed in Section II, we will simulate the PERC (passivated emitter and rear cell) solar cells as described below with various emitter and inactive P profiles to give a perspective of what can be achieved with PSG processes and to show an upper limit for a nearly ideal emitter (optimized Gaussian shaped emitter for the simulated PERC cell).

A. Simulation model details

A PERC solar cell[47] is simulated in Sections III B and IV to discuss different aspects of emitters fabricated with a PSG layer. The specifications are as follows: The simulated PERC solar cell is 180 μm thick and is simulated in the unit domain shown in Ref. 48. A distance of 1.2 mm is assumed between the front grid finger contacts, which have a width of 45 μm. Three rear-finger contacts are placed between two front contacts, which have a width of 90 μm. We assume a rear surface recombination velocity $S_{rear} = 10$ cm/s at the rear passivation, a value which has been experimentally realized with Al_2O_3, e.g., in Ref. 49. The B doping in the base is 2 Ωcm, equivalent to a B concentration of $7.12 \times 10^{15}\,cm^{-3}$. All cells have the same local Al-BSF[50] (back surface field) covering the rear finger-shaped contacts. The Si bulk SRH lifetime is set to 1 ms, assuming high-quality Cz Si material in a deactivated state of the B-O complex. SRH recombination due to inactive P is modeled with parameters from Ref. 12. The remaining model parameters for Si, such as band diagram parameters and recombination models, are taken from Ref. 48 (including Fermi–Dirac statistics and Schenk's band gap narrowing model).

All simulations are carried out at 1 Sun and 300 K, using the software Sentaurus TCAD (Version C-2012.06, from Synopsys, Inc.). The optical generation within the textured wafers is modeled by ray tracing using the software Sunrays.[51] The resulting IV-curves are corrected by metal shading and resistive losses in the metalization that are typical for $15.6 \times 15.6\,cm^2$ solar cells.

To show the effect of the emitter and inactive P on the described PERC solar cell, several emitters and inactive P profiles from the literature are used. First, the profiles from Fig. 4 are used. Similar results were observed by Lee *et al.*,[14] where lowering the $POCl_3$ flow rate results in lower inactive P concentrations in Si. Khandelwal *et al.*[15] show that after removing the PSG and performing an additional drive-in (oxidation) step, the inactive P can be resolved entirely. Prajapati *et al.*[16] also show that additional drive-in steps (oxidations) can decrease or entirely dissolve the inactive P in Si. Cabrera *et al.*[52] present two possible PSG diffused emitters where the amount of inactive P is reduced significantly in one case. Our work[53] presents an optimized emitter profile including lower inactive P concentration.

Bentzen *et al.*[42] present a model that simulates the inactive P and the emitter from a fixed surface concentration. In this model, the variation of the $POCl_3$ flow is only included empirically by a variation of the P concentration at the PSG/Si interface. As we know the P concentration from our experiments, the model is used here to simulate both profiles. Using the above experimental results, we vary the surface concentration from $5 \times 10^{19}\,cm^{-3}$ to $7.5 \times 10^{20}\,cm^{-3}$ and keep the diffusion process constant at 840 °C and 30 min, followed by a ramp down to 500 °C in steps of 17 K/min. As ideal emitter we choose a Gaussian profile with a peak concentration of $1 \times 10^{19}\,cm^{-3}$, a depth of 0.4 μm, and an ideal front surface recombination velocity s_{front} of 1 cm/s. The s_{front} values for emitters without inactive P are taken from Ref. 54, and the s_{front} values for emitters containing inactive P from Ref. 12. The additional SRH recombination due to inactive P is simulated using the capture cross sections from Ref. 12. The inactive P and emitter profiles from all the above-listed references are used to simulate the PERC solar cells as described above. It should be noted that only the emitter and inactive P profiles are varied, and all other parameters are held constant.

B. Simulation results

Figure 5 shows results of simulated PERC solar cells with different emitters and inactive phosphorus profiles as explained in Section III A. Plotted are the cell efficiency η as a function of open-circuit voltage V_{OC} and η as a function of short-circuit current density J_{SC}. The dashed line represents the boundary between emitters with and without inactive P. In general, the following conclusions can be drawn: With decreasing inactive P concentration, the SRH recombination in the emitter region decreases and consequently V_{OC} and η increase. Further increase in V_{OC} is due to lower peak concentrations of the electrically active profile (emitter) and, with this, the lowering of Auger recombination. Additionally, the surface recombination velocity is reduced with lower peak concentration. The ideal emitter represents hereby an upper limit.

J_{SC} shows the same general trends. With decreasing the inactive P concentration, J_{SC} increases due to a better collection efficiency of photo-generated carriers (better blue response). Further increase is possible due to lower Auger recombination rates. Because the collection efficiency of highly-doped emitters depends sensitively on their dopant profile and their profile of inactive P, the simulated J_{sc} values scatter to some extent.

Based on these results, the optimal strategy would be to reduce the inactive P concentration as much as possible and in addition lower the peak concentration of the electrically active emitter. As mentioned earlier, this simple approach has two problems. First, the gettering efficiency of the

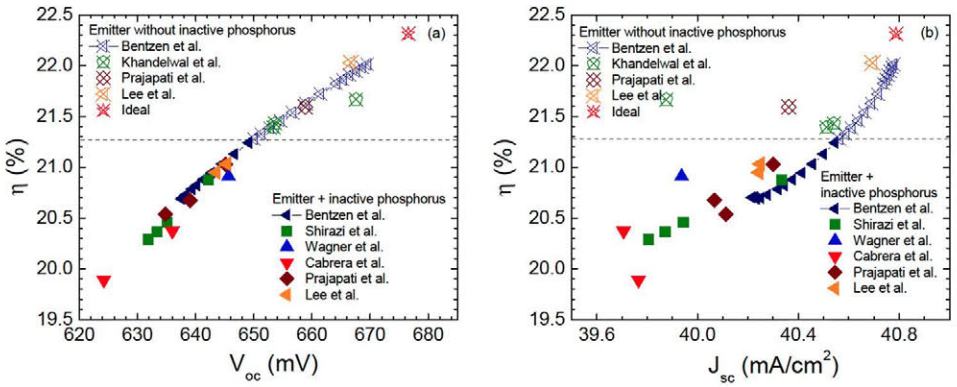

FIG. 5. Simulated I-V-curve parameters from PERC solar cells using various P emitter dopant profiles and inactive P profiles from the literature as indicated. (a) Cell efficiency η over V_{OC}; the PERC cells without inactive P have a higher η due to lower SRH recombination. (b) A similar trend can be observed in J_{SC} over η; the inactive P lowers the collection probability of photogenerated carriers and reduces J_{SC}.

emitter may be reduced. Second, contact formation may pose a serious problem. We are going to show limitations of these two issues in Sections IV–V.

IV. DEFECT GETTERING WITH THE PSG PROCESS

The in-diffusion of P into Si from a PSG layer is strongly coupled to the gettering process. Impurities pile up under the in-diffused P profile, while the recombination activity of these gettered impurities is strongly reduced in the emitter region as mentioned in Section I. Consequently, the Si bulk lifetime increases. Section III showed that lowering the P peak concentration in Si is an effective way to increase PERC solar cell efficiency. We will show now that gettering may become inefficient if the peak concentration of P is significantly reduced. We perform another simulation study, using Fe as a representative impurity which is well known to limit solar cell performance.[55] See Refs. 56–58 for comprehensive review of several models of iron impurity evolution during solar cell processing.

The gettering of Fe is simulated with the Impurity-to-Efficiency simulator[59,60] where the simulated P in-diffusion is based on the model from Bentzen *et al.*[42] and the Fe segregation in the P layer on the one developed by Haarahiltunen *et al.*[61] We assume an initial homogeneous contamination of interstitial iron (Fe_i) in the Si bulk material of $1.0 \times 10^{11}\,cm^{-3}$ and a total iron concentration Fe of $1.0 \times 10^{13}\,cm^{-3}$. The initial radius of the Fe precipitates is set to 25 nm, within the range of sizes that have been observed experimentally in mc-Si.[62,63] For a representative PSG process we simulate the following diffusion and gettering scenario. The process occurs at 840 °C for 30 min, with a variable cool down ramp in 5, 10, 15, …, 100 min to 500 °C, which corresponds to 68 K/min (5 min) to 3.4 K/min (100 min). In addition, the P peak concentration was varied to simulate a reduction of P in the PSG. We simulated a peak concentration of $7.5 \times 10^{20}\,cm^{-3}$ including inactive P and peak concentrations of $2.5 \times 10^{20}\,cm^{-3}$, $1.0 \times 10^{20}\,cm^{-3}$, and $5.0 \times 10^{19}\,cm^{-3}$ without inactive P. A potential deactivation of part of the P during the slow ramps is considered not to be significant as compared with the other factors influencing the gettering process. The resulting emitter and inactive P profiles are implemented in the PERC solar cells as described in Section III.

The results are shown in Fig. 6. Plotted is the efficiency η of the PERC cells over the average bulk Fe_i concentration in Si after gettering. This average Fe_i concentration is the average in bulk Si, as simulated from 2 μm to 180 μm depth, which excludes the pile-up of Fe_i in the emitter region. In general, the following statements can be drawn. First, the cool-down ramp rate is highly important for the gettering efficiency. A slower cool down leads to a better gettering of Fe_i, which means lower Fe_i bulk concentration for all peak concentrations. These trends have also been observed experimentally, for example, in Refs. 64–66. A very fast cool down can result in even higher Fe_i concentrations after the gettering process. This can be explained as follows. During the process, e.g., at 840 °C, Fe_i approaches its solubility limit in Si and will segregate to the emitter region. During a slow cool down, the solubility limit is decreasing slowly, giving Fe_i the opportunity to diffuse to the emitter region or precipitate in the bulk. During a fast cool down the fast reduction of temperature precludes that Fe_i can diffuse to the emitter region or to a precipitate, leading to a Fe_i concentration in the base that is even higher than that of the as-grown state.

Second, with decreasing P peak concentrations, gettering is weaker because the gettering efficiency is coupled to

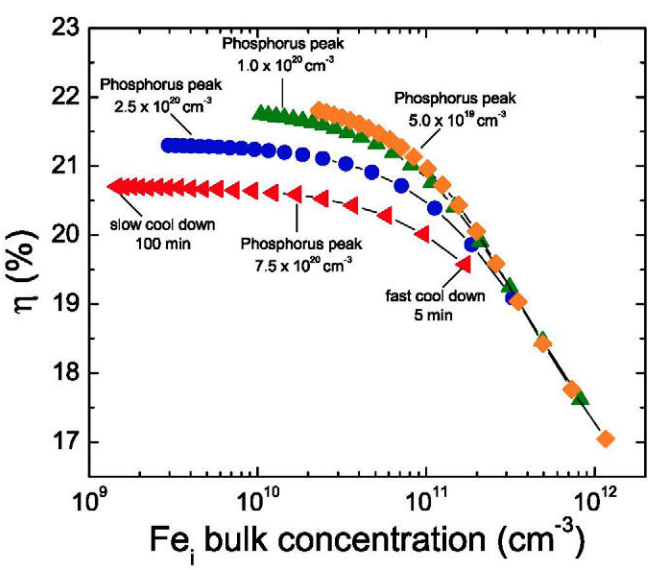

FIG. 6. Simulated PERC solar cell efficiencies for different emitter peak concentrations and cool down rates during P gettering. Plotted is the efficiency η over the average Fe_i concentration in the Si bulk after gettering. Each line represents the situation for a specific P peak, and each symbol represents a different cooling rate. Symbols on the very left have a slow cool down rate, 100 min (3.4 K/min) from 840 °C to 500 °C, while symbols on the right side have a fast cool down rate, 68 K/min (in 5 min) from 840 °C to 500 °C.

the P peak concentration. This effect has also been observed experimentally.[67,68] Consequently, a longer cool down is needed to achieve the same Fe_i concentration.

Other impurities, such as Ag, Ti, Mn, Co, Cr, Ni, Mo, and Cu, are gettered during P diffusion as well.[21–24] These impurities might behave similarly to Fe_i, according to their respective diffusivity and solubility limit values, and the ability to getter them may also depend on the cooling rate and peak concentration of P, among other factors. Note that part of the impurities can re-diffuse into the base region during the final firing step, which is not taken into account here.

In summary, if the P concentration in the PSG is significantly lowered, higher efficiencies are possible due to lower inactive P and lower Auger and surface recombination velocities, but gettering could be less efficient. Longer cool down ramps may enable co-optimization of inactive P concentration and impurity gettering.

V. CONTACT FORMATION AND PSGs

As outlined in the introduction, the metal contact formation by screen-printing is still a subject of investigation. In general, contacts to emitters with a low concentration of inactive phosphorus may suffer from high contact resistivities (larger than 4 m Ω cm^2) causing low fill factors (FF) of the IV curve. In this section, we focus on the lower limits of electrically inactive P concentration.

To investigate the influence of the inactive P on contact formation, we processed solar cells having several different densities of inactive P in their emitter, as shown in Fig. 4. After alkaline texturization and cleaning, several $POCl_3$ diffusion processes have been applied by adjusting the $POCl_3$-N_2 gas flow during the pre-deposition phase, as discussed in Section III. The flow was varied in three different rates: 250, 375, and 500 sccm for five samples each. Afterward, the PSG was removed by Hydrofluoric acid, and a 70 nm thick layer of PECVD SiN_x with a refractive index of 2.0 at a wavelength of 633 nm was deposited on the front side. The metalization was realized by a standard screen-printing procedure with a 3-busbar front side design. The rear side was metalized with a full-area thick-film Al paste to form the Al-BSF. The base material for this study is Cz boron-doped (100) silicon wafers with a base resistivity of 2.7 Ω cm and a thickness of 170 μm.

Fig. 7 shows the results. Plotted are the fill factor and series resistance R_s over the $POCl_3$ flow. With decreasing $POCl_3$, the *FF* drops because R_s increases. Microscopic investigations in Ref. 31 indicate that a concentration between approximately 5×10^{20} cm^{-3} and 7×10^{20} cm^{-3} of inactive P is necessary to form a high-quality contact. Already years ago, very lightly doped emitters with a surface P concentration as low as 4.0×10^{19} cm^{-3} could be contacted with affordable contact resistivities.[32] From recent screen-printing pastes it is reported[31] that the Ag crystallite density is independent of the emitter doping, but the Ag crystallite size increases as a function of the thickness of the plateau. This might be because emitters with a short plateau are likely to be etched by the Ag paste and this might generally lead to contact problems, which could explain the low *FF* when strongly lowering the $POCl_3$ flow (this was not the case in the cells investigated here). Another general possibility is that with decreasing P the in-diffused Ag profile might overcome the P profile, shunting the emitter region.[28] However, a detailed study[69] showed that this effect is not expected to be significant in the emitters discussed here. A further possibility may be the onset of band bending at the interface between Si and the PbO glass layer of the screen-printed contact.[30] In summary, while the P density at the Si surface is not anymore the limiting factor for contacting with low contact resistivity, care must be taken in experiments and in mass production that the emitter is sufficiently deep beneath the contacts. We take this into account in the proposed design of a high-efficiency emitter in Section VI.

VI. HIGH-EFFICIENCY EMITTER FABRICATED WITH PSG

Fig. 3(b) indicates that, with varying the $POCl_3$ flow, only a limited change in the P concentration in the PSG layer seems possible. On the other hand, we also show that such a limited change in P concentration in the PSG layer strongly determines the resulting dopant profile in Si (cf. Fig. 4) and in many circumstances causes a significant amount of inactive P. The question arises, whether it is at all possible with $POCl_3$ to form a high efficiency emitter, like one that is close to the emitter implemented in PERL (passivated emitter, rear locally diffused) cells having efficiencies of up to 25%.[70] The n^+ part of the emitter in these cells has a Gaussian shape with a very low peak concentration at the surface of $N_{peak} = 5.0 \times 10^{18}$ cm^{-3} but a considerable junction depth of $d_j = 1$ μm, resulting in a sheet resistivity near $\rho_{sh} = 200$ Ω/sq and a saturation current J_0 near 6 fA/cm^2. Our simulations

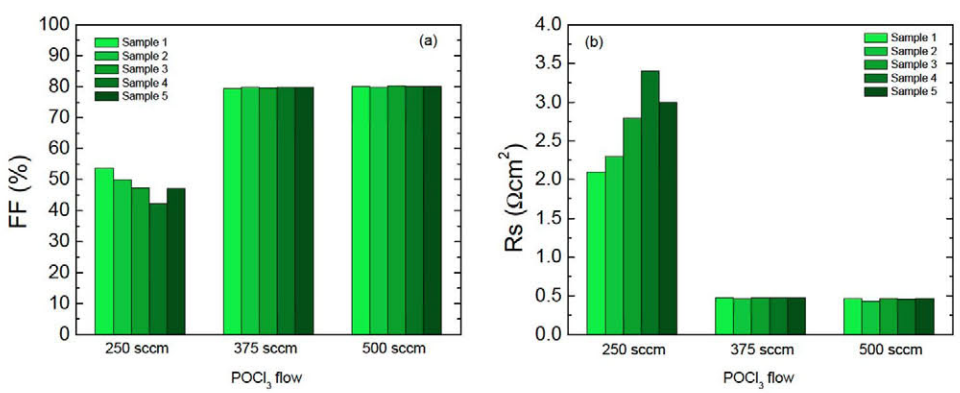

FIG. 7. Fill factor and series resistance of solar cells as a function of $POCl_3$ flow rate. Using standard screen-printing Ag paste and firing profiles, an adequate contact cannot be formed with low $POCl_3$ flows and leads to a dramatic decrease in the fill factor.

with Bentzen's model[42] show that such an emitter would require diffusion times longer than one hour and therefore too long for standard mass production. Our simulations predict, however, that an emitter with $N_{peak} = 8.0 \times 10^{18}\,cm^{-3}$ and $d_j = 0.4\,\mu m$ comes very close to the PERL emitter, resulting in $\rho_{sh} = 380\,\Omega/sq$ and a J_0 below 10 fA/cm^2 if passivated with a stack of a thin SiO_2 capped with a usual PECVD SiN_x layer. This P profile requires a diffusion process at 860 °C for 60 min instead of conventional 840 °C for 30–40 min. During these 60 min, the SiO_2 layer of Fig. 2(a) may form a diffusion barrier for P. Nevertheless, there is a sufficient amount of P available for in-diffusion.

To be contacted, the PSG layer must be locally laser-fired[71] before removal to form the n^{++} region, as for example, described in Ref. 72. The width of this n^{++} region depends on the alignment tolerances but is typically 150 μm wide. Our simulations predict a minimum J_0 of 215 fA/cm^2 in the metalized part and a J_0 near 80 fA/cm^2 (Auger limit) in the passivated part of the n^{++} region if the laser-induced defect density is insignificant. Afterward, the entire emitter (including the laser-fired part) must be homogeneously etched back by 240 nm to remove the highly doped region near the textured surface and all the inactive P, and is subsequently passivated.[73,74] This approach also enables the PSG to getter impurities sufficiently, because the peak concentration before etch-back is adequately high. The predicted optimum finger pitch is 900 μm for 30 μm wide and 15 μm high metal fingers, and in this case J_0 of the entire emitter (n^+ and n^{++} part) is predicted to be 25 fA/cm^2. Hence, our process and device simulations suggest that a high-efficiency emitter is indeed possible with $POCl_3$ diffusion in mass production if a suitable metalization can be achieved.[15,75]

VII. CONCLUSIONS

With applying numerical simulations, it is possible to combine various experimental findings into a model, such as the composition of the phosphorus rich glass (PSG), inactive phosphorus in Si and its distribution, the gettering ability, and metal contact formation. Such a detailed model allows us to make specific forecasts that with slightly different PSG process times and temperatures (860 °C for 60 min) an emitter with a saturation current density of only 25 fA/cm2 can be achieved (10 fA/cm2 in the lowly doped part and 80 fA/cm2 in the highly doped part). Hereby the gettering ability even for multicrystalline Si is sufficiently strong to be suitable for solar cells (down to peak dopant concentrations of $5 \times 1019\,cm^{-3}$). More critical remains the question if emitters with low content of inactive P can be contacted with sufficiently low contact resistivities (below 4 m Ω cm^2). As possible well-known solution we suggest an additional laser doping from the PSG layer for increasing the dopant concentration at the metal contacts, followed by a homogeneous etch-back of the emitter.

ACKNOWLEDGMENTS

We thank Dr. Pavel Fastenko, Dr. Nelson Braga, Dr. Pratheep Balasingam, and Dr. Terry Ma of Synopsys, Inc., for enabling the development of the I2E Model in the Alagator Scripting Language and its use with Sentaurus TCAD. This work was supported by the U.S. National Science Foundation (NSF) and the U.S. Department of Energy under NSF CA No. EEC-1041895 and by the U.S. Department of Energy under Award No. DE-EE0006335. C. del Cañizo acknowledges the support of the Department of Mechanical Engineering at the Massachusetts Institute of Technology through the Peabody Visiting Professorship, and the Comunidad de Madrid through the MADRID-PV S2013/MAE-2780 project. A. E. Morishige acknowledges the support of the Department of Defense through the NDSEG fellowship program.

[1]P. Pichler, *Intrinsic Point Defects, Impurities, and Their Diffusion in Silicon* (Springer Science and Business Media, 2012).
[2]S. Solmi, A. Parisini, R. Angelucci, A. Armigliato, D. Nobili, and L. Moro, Phys. Rev. B **53**, 7836 (1996).
[3]B. Giessen and R. Vogel, Z. Metallk. **50**, 274 (1959).
[4]P. Negrini, D. Nobili, and S. Solmi, J. Electrochem. Soc. **122**, 1254 (1975).
[5]D. Nobili, A. Armigliato, M. Finnetti, and S. Solmi, J. Appl. Phys. **53**, 1484 (1982).
[6]A. Bourret and W. Schröter, Ultramicroscopy **14**, 97 (1984).
[7]L. Morettini and D. Nobili, Mater. Chem. Phys. **10**, 21 (1984).
[8]S. T. Dunham, J. Electrochem. Soc. **142**, 2823 (1995).
[9]A. Armigliato, D. Nobili, S. Solmi, G. Blendin, B. Schum, A. Lachowicz, and J. Horzel, Sol. Energy Mater. Sol. Cells **95**, 3099 (2011).
[10]P. Ostoja, S. Guerri, P. Negrini, and S. Solmi, Sol. Cells **11**, 1 (1984).
[11]B. Min, H. Wagner, A. Dastgheib-Shirazi, and P. P. Altermatt, Energy Proc. **55**, 115 (2014).
[12]B. Min, H. Wagner, A. Dastgheib-Shirazi, A. Kimmerle, H. Kurz, and P. P. Altermatt, Phys. Status Solidi RRL **8**, 680 (2014).
[13]A. Dastgheib-Shirazi, M. Steyer, G. Micard, H. Wagner, P. P. Altermatt, and G. Hahn, Energy Proc. **38**, 254 (2013).
[14]H. J. Lee, M. G. Kang, S. J. Choi, G. H. Kang, J. M. Myoung, and H.-E. Song, Curr. Appl. Phys. **13**, 1718 (2013).
[15]R. Khandelwal, H. Windgassen, J. van Molken, T. M. Pletzer, and H. Kurz, in *Proceedings of the 39th IEEE Photovoltaic Specialists Conference* (Tampa, FL, 2013), p. 2217.
[16]V. Prajapati, J. Horzel, P. Choulat, T. Janssens, J. Poortmans, and R. Mertens, in *Proceedings of the 27th European Photovoltaic Solar Energy Conference and Exhibition* (Frankfurt, Germany, 2012), p. 680.
[17]G. Masetti, D. Nobili, S. Solmi, H. Huff, and E. Sirtl, in *Proceedings of the Electrochemical Society* (Princeton, NJ, 1977), p. 648.
[18]A. Carabelas, D. Nobili, and S. Solmi, J. Phys. Coll. **43**(C1) 187 (1982).
[19]P. J. Richter, F. J. Bottari, and D. C. Wong, in *Proceedings of the 35th IEEE Photovoltaic Specialists Conference* (Honolulu, Hawaii, 2010), p. 003593.
[20]J. Kang and D. Schroder, J. Appl. Phys. **65**, 2974 (1989).
[21]D. Macdonald, A. Cuevas, A. Kinomura, and Y. Nakano, in *Proceedings of the 29th IEEE Photovoltaic Specialists Conference* (New Orleans, LA, 2002), p. 285.
[22]A. Bentzen, A. Holt, R. Kopecek, G. Stokkan, J. Christensen, and B. Svensson, J. Appl. Phys. **99**, 093509 (2006).
[23]M. B. Shabani, T. Yamashita, and E. Morita, ECS Trans. **16**, 179 (2008).
[24]M. A. Jensen, J. Hofstetter, A. E. Morishige, G. Coletti, B. Lai, D. P. Fenning, and T. Buonassisi, Appl. Phys. Lett. **106**, 202104 (2015).
[25]J. Hofstetter, D. P. Fenning, D. M. Powell, A. E. Morishige, H. Wagner, and T. Buonassisi, IEEE J. Photovoltaics **4**, 1421 (2014).
[26]R. J. S. Young and A. F. Carroll, in *Proceedings of the 16th European Photovoltaic Solar Energy Conference and Exhibition* (Glasgow, Scotland, 2000), p. 1731.
[27]C. Ballif, D. M. Huljić, G. Willeke, and A. Hessler-Wyser, Appl. Phys. Lett. **82**, 1878 (2003).
[28]M. M. Hilali, A. Rohatgi, and S. Asher, IEEE Trans. Electron Devices **51**, 948 (2004).
[29]Z. G. Li, L. Liang, and L. K. Cheng, J. Appl. Phys. **105**, 066102 (2009).
[30]H. Mackel and P. P. Altermatt, IEEE J. Photovoltaics **5**, 1034 (2015).
[31]E. Cabrera, S. Olibet, D. Rudolph, P. E. Vullum, R. Kopecek, D. Reinke, C. Herzog, D. Schwaderer, and G. Schubert, Prog. Photovoltaics **23**, 367 (2015).

[32]G. Schubert, F. Huster, and P. Fath, Sol. Energy Mater. Sol. Cells **90**, 3399 (2006).
[33]M. Steyer, A. Dastgheib-Shirazi, H. Wagner, G. Micard, P. Altermatt, and G. Hahn, in *Proceedings of the 27th European Photovoltaic Solar Energy Conference and Exhibition* (Frankfurt, Germany, 2012), p. 1325.
[34]J. Dathe, W. Müller, and L. Grasser, Z. Angew. Phys. **30**, 272 (1970).
[35]A. Dastgheib-Shirazi, M. Steyer, G. Micard, H. Wagner, P. Altermatt, and G. Hahn, in *Proceedings of the 38th IEEE Photovoltaic Specialists Conference* (Austin, TX, 2012), p. 1584.
[36]M. Steyer, A. Dastgheib-Shirazi, G. Micard, H. Wagner, P. P. Altermatt, and G. Hahn, in *Proceedings of the 29th European Photovoltaic Solar Energy Conference and Exhibition* (Amsterdam, The Netherlands, 2014), p. 1104.
[37]R. Chen, H. Wagner, A. Dastgheib-Shirazi, M. Kessler, Z. Zhu, V. Shutthanandan, P. P. Altermatt, and S. T. Dunham, J. Appl. Phys. **112**, 124912 (2012).
[38]K. Sakamoto, K. Nishi, F. Ichikawa, and S. Ushio, J. Appl. Phys. **61**, 1553 (1987).
[39]R. Ghoshtagore, Thin Solid Films **25**, 501 (1975).
[40]M. Rauer, M. Rüdiger, C. Schmiga, H. Strutzberg, M. Bähr, M. Glatthaar, and S. W. Glunz, J. Appl. Phys. **114**, 203702 (2013).
[41]Y. Komatsu, A. H. Vlooswijk, P. R. Venema, and I. G. Romijn, Energy Proc. **55**, 241 (2014).
[42]A. Bentzen, A. Holt, J. Christensen, and B. Svensson, J. Appl. Phys. **99**, 064502 (2006).
[43]D. Klaassen, Solid-State Electron. **35**, 953 (1992).
[44]D. Klaassen, Solid-State Electron. **35**, 961 (1992).
[45]P. Balk and J. Eldridge, Proc. IEEE **57**, 1558 (1969).
[46]T. Aoyama, H. Tashiro, and K. Suzuki, J. Electrochem. Soc. **146**, 1879 (1999).
[47]A. W. Blakers, A. Wang, A. M. Milne, J. Zhao, and M. A. Green, Appl. Phys. Lett. **55**, 1363 (1989).
[48]P. P. Altermatt, J. Comput. Electron. **10**, 314 (2011).
[49]B. Veith, F. Werner, D. Zielke, R. Brendel, and J. Schmidt, Energy Proc. **8**, 307 (2011).
[50]S. Kluska and F. Granek, IEEE Electron Device Lett. **32**, 1257 (2011).
[51]R. Brendel, in *Proceedings of the 12th European Photovoltaic Solar Energy Conference* (Amsterdam, The Netherlands, 1994), p. 1339.
[52]E. Cabrera, S. Olibet, D. Rudolph, P. E. Vullum, R. Kopecek, D. Reinke, C. Herzog, D. Schwaderer, and G. Schubert, Prog. Photovolt: Res. Appl. **23**, 367–375 (2015).
[53]H. Wagner, A. Dastgheib-Shirazi, R. Chen, S. T. Dunham, M. Kessler, and P. P. Altermatt, in *Proceedings of the 37th IEEE Photovoltaic Specialists Conference* (Seattle, WA, 2011), p. 002957.
[54]P. P. Altermatt, J. O. Schumacher, A. Cuevas, M. J. Kerr, S. W. Glunz, R. R. King, G. Heiser, and A. Schenk, J. Appl. Phys. **92**, 3187 (2002).
[55]B. Sopori, J. Electron. Mater. **31**, 972 (2002).
[56]A. Morishige, H. Laine, J. Schön, A. Haarahiltunen, J. Hofstetter, C. del Cañizo, M. Schubert, H. Savin, and T. Buonassisi, Appl. Phys. A **120**, 1357 (2015).
[57]S. P. Phang and D. Macdonald, IEEE J. Photovoltaics **4**, 64 (2014).
[58]J. Schön, V. Vähänissi, A. Haarahiltunen, M. C. Schubert, W. Warta, and H. Savin, J. Appl. Phys. **116**, 244503 (2014).
[59]J. Hofstetter, D. Fenning, M. Bertoni, J. Lelièvre, C. D. Cañizo, and T. Buonassisi, Prog. Photovoltaics **19**, 487 (2011).
[60]A. E. Morishige, H. Wagner, J. Hofstetter, I. Avci, C. del Cañizo, and T. Buonassisi, Energy Proc. **77**, 119 (2015).
[61]A. Haarahiltunen, H. Savin, M. Yli-Koski, H. Talvitie, and J. Sinkkonen, J. Appl. Phys. **105**, 023510 (2009).
[62]D. Fenning, J. Hofstetter, M. Bertoni, S. Hudelson, M. Rinio, J. Lelievre, B. Lai, C. Del Canizo, and T. Buonassisi, Appl. Phys. Lett. **98**, 162103 (2011).
[63]D. P. Fenning, J. Hofstetter, M. I. Bertoni, G. Coletti, B. Lai, C. Del Canizo, and T. Buonassisi, J. Appl. Phys. **113**, 044521 (2013).
[64]P. Manshanden and L. Geerligs, Sol. Energy Mater. Sol. Cells **90**, 998 (2006).
[65]J. Hofstetter, J. F. Lelievre, C. del Cañizo, and A. Luque, Solid State Phenom. **156–158**, 387 (2010).
[66]D. P. Fenning, J. Hofstetter, A. E. Morishige, D. M. Powell, A. Zuschlag, G. Hahn, and T. Buonassisi, Adv. Energy Mater. **4**, 1400459 (2014).
[67]A. Peral, A. Dastgheib-Shirazi, H. Wagner, G. Hahn, and C. del Cañizoa, in *Proceedings of the 5th International Conference on Crystalline Silicon Photovoltaics* (Constance, Germany, 2015).
[68]M. Syre, S. Karazhanov, B. Olaisen, A. Holt, and B. Svensson, J. Appl. Phys. **110**, 024912 (2011).
[69]R. Hoenig, A. Kalio, J. Sigwarth, F. Clement, M. Glatthaar, J. Wilde, and D. Biro, Sol. Energy Mater. Sol. Cells **106**, 7 (2012).
[70]J. Zhao, A. Wang, M. A. Green, and F. Ferrazza, Appl. Phys. Lett. **73**, 1991 (1998).
[71]C. Carlsson, A. Esturo-Breton, M. Ametowobla, J. Köhler, and J. Werner, in *Proceedings of the 21st European Photovoltaic Solar Energy Conference and Exhibition* (Dresden, Germany, 2006), p. 938.
[72]Z. Hameiri, L. Mai, T. Puzzer, and S. R. Wenham, Sol. Energy Mater. Sol. Cells **95**, 1085 (2011).
[73]H. Haverkamp, A. Dastgheib-Shirazi, B. Raabe, F. Book, and G. Hahn, in *Proceedings of the 33rd IEEE Photovoltaic Specialists Conference* (San Diego, CA, 2008), p. 1.
[74]S. Eisele, T. C. Röder, J. R. Köhler, and J. H. Werner, Appl. Phys. Lett. **95**, 133501 (2009).
[75]A. Wolf, A. Kimmerle, S. Werner, S. Maier, S. Belledin, S. Meier, and D. Biro, in *Proceedings of the 31st European Photovoltaic Solar Energy Conference and Exhibition* (Hamburg, Germany, 2015).